International Journal of Pharmaceutics 592 (2021) 120057

Contents lists available at ScienceDirect

International Journal of Pharmaceutics

journal homepage: www.elsevier.com/locate/ijpharm

Cocrystals to tune oily vitamin E into crystal vitamin E

Bingqing Zhu, Qi Zhang, Liye Lu, Junjie Bao, Xiaoyi Rong, Jian-Rong Wang, Xuefeng Mei *

Pharmaceutical Analytical & Solid-State Chemistry Research Center, Shanghai Institute of Materia Medica, Chinese Academy of Sciences, Shanghai 201203, China

ARTICLE INFO

Keywords:
Cocrystal
Vitamin E
Solidification
Stability
Bioavailability

ABSTRACT

d-α-tocopherol (**d-αToc**), the most biologically active form of natural Vitamin E, is oily in appearance and unstable to oxygen. Esterification and encapsulation are generally needed to stabilize and solidify **d-αToc** for the purpose of its expanding applications. In this study, we propose a more effective way to stabilize and solidify **d-αToc** oil in one step. By cocrystallization, the melting point of **d-αToc** is significantly increased, such that the oily **d-αToc** is successfully transformed into solid form at room temperature. The single crystal structure of **d-αToc** was firstly uncovered and the molecular interaction in cocrystals was revealed. Crystalline Vitamin E shows high stability to light and temperature. Its spherical crystallization affords good powder flowability, which is extremely important as food or feed additives. Moreover, cocrystal Vitamin E remains the original form of tocopherol without esterification and thus has a great advantage on higher bioavailability. Cocrystallization of oily **d-αToc** spares the use of acetic ester and a mass of excipients, which is of great environmental importance and greatly reduces the production cost.

1. Introduction

Since its discovery over 90 years ago, Vitamin E has been widely used in food and feed industry as an essential nutrient. Due to its antioxidant property, it also provides additional health benefits in diseases associated with oxidative stress, such as cardiovascular disease, chronic inflammation (El Hadi et al., 2018; Sebastian Larion and Sandeep Khurana, 2018), and neurologic disorders (Mangialasche et al., 2013; Ulatowski et al., 2014). Naturally occurring Vitamin E is extracted from plant oils, usually soybean oil or sunflower oil. It is composed of eight family members (α-, β-, γ-, δ-tocopherol and the tocotrienols), wherein RRR-α-tocopherol (**d-αToc**, Fig. 1) is chemically and biologically the most efficient one. However, **d-αToc** is highly unstable to oxidation and may lose its efficacy during the processing and storage (Player et al., 2006; Lv et al., 2019). To maintain stability, most commercially available **d-αToc** has been structurally modified with acetate or succinate, but at the same time, sacrificing the antioxidant capability of **d-αToc** *in vitro*. What's more, the esterified form needs to be hydrolyzed first in gastrointestinal tract before it can be absorbed (Reboul, 2017), which decreases its bioavailability (Desmarchelier et al., 2013; Bruno et al., 2006). In addition to chemical stability, another challenge of incorporating Vitamin E into commercial products is that **d-αToc** and even its acetated form is oily in physical appearance with high viscosity, which makes them more difficult to be handled. To address this problem, encapsulation technology is used to convert oil into powder (Gangurde et al., 2016). This technology has also been applied to many other unstable vitamins, like Vitamin A, Vitamin K_2 and Vitamin D_3. However, the loading of the active compounds is limited by encapsulation efficiency and a large amount of excipients (usually starch or gelatin) without any nutritional function are introduced. For Vitamin E, the loading of **d-αToc acetate** in commercially available Vitamin E products is 50% at most, and there is still a potential risk of oil leakage during heating or compression. The combination of esterification and encapsulation to stabilize and solidify Vitamin E oil is complicated and lose the nature essence of **d-αToc** by changing its chemical structure. Herein, we propose a more straightforward and effective way to develop **d-αToc** powder without sacrificing its natural attributes.

Cocrystals, as an emerging class of solid form, have continued to gain attention due to its ability to modulate many physicochemical properties of a compound without altering its chemical structure (Duggirala et al., 2016). We have previously studied on the stability improvement of Vitamin D_3 and Vitamin K_3 through cocrystallization (Wang et al., 2016; Zhu et al., 2016). In this study, we turn to the challenges of Vitamin E formulation. There have been a few cases of tuning liquid/oily state into solid state through cocrystallization, which was proved to be a practical and promising method. Aakeroy et al. developed a simple protocol to convert iodoperfluoroalkanes into stable crystalline materials using halogen-bond driven cocrystallization (Aakeroy et al., 2015). Florene

* Corresponding author.
E-mail address: xuefengmei@simm.ac.cn (X. Mei).

https://doi.org/10.1016/j.ijpharm.2020.120057
Received 9 September 2020; Received in revised form 22 October 2020; Accepted 3 November 2020
Available online 7 November 2020

et al. obtained a novel solid form of the liquid anesthetic propofol, with a melting point of 50 °C higher than the starting material (McKellar et al., 2014). However, in the case of **d-αToc**, high conformational flexibility of the long alkyl chain poses extra difficulty in crystallization. Strong molecular interactions are needed to be introduced to overcome the mobility and achieve the conformational stability of the alkyl chain. Herein, we reported on the crystal engineering of oily **d-αToc** and successfully obtained three cocrystals.

2. Material and methods

2.1. Materials

The sample of **d-αToc** used in the present work was purchased from Shandong New Element Biotechnology Co., Ltd. The coformers and all analytical grade solvents were purchased from Sinopharm Chemical Reagent Company and used without further purification.

2.2. Preparation of cocrystal *d-αToc·DPE*

86 mg **d-αToc** (0.2 mmol) and 18.2 mg **DPE** (0.1 mmol) were dissolved in 0.5 mL mixture solvent of methanol and acetone. The solution was filtered and cooled at −20 °C. After two days, plate single crystals were obtained.

2.3. Preparation of cocrystal *d-αToc·L-Pro*

4.3 g (10 mmol) **d-αToc** and 0.575 g (5 mmol) **L-Pro** were dissolved into 10 mL methanol and the solution was cooled at −20 °C. Bulk white powder was precipitated, which was then filtered and dried in vacuum at room temperature. The yield was about 95%.

2.4. Preparation of cocrystal *d-αToc·Bet*

4.3 g (10 mmol) **d-αToc** and 0.585 g (5 mmol) **Bet** were dissolved into 10 mL methanol and the solution was cooled at −20 °C. Bulk white powder was precipitated, which was then filtered and dried in vacuum at room temperature. The yield was about 95%.

2.5. Powder X-ray diffraction (PXRD)

PXRD patterns were collected using a Bruker D8 Advance X-ray diffractometer (Cu Kα radiation). Voltage and current of the generator were set to 40 kV and 40 mA, respectively. Data over the range 3–40 ° 2θ was collected with a scan rate of 5°/min at ambient temperature. Data were imaged and integrated with RINT Rapid and peak-analyzed with Jade 6.0 from Rigaku.

2.6. Single crystal X-ray diffraction (SCXRD)

X-ray diffractions of the single crystal were carried out at 170 K and 303 K on a Bruker Apex II CCD diffractometer using Mo-Kα radiation (λ = 0.71073 Å). Integration and scaling of intensity data was performed using the SAINT program (Sheldrick, 1995). Data were corrected for the effects of absorption using SADABS (Sheldrick, 1997). The structures were solved by direct method and refined with full-matrix least-squares technique using SHELX-2014 software (Sheldrick, 2015). Non-hydrogen atoms were refined with anisotropic displacement parameters, and hydrogen atoms were placed in calculated positions and refined with a riding model. In the case of the crystal structure at 303 K, due to the great dynamic at higher temperature, the long alkyl chain can not be determined and leads to a large disorder. Crystallographic data are summarized in Table S1. The data can be obtained free of charge via www.ccdc.cam.ac.uk/data_request/cif.

2.7. Differential scanning calorimetry (DSC)

DSC experiments were performed on a TA Q2000 instrument under nitrogen gas flow of 20 mL min^{-1} purge. Ground samples weighting 3–5 mg were heated in sealed non-hermetic aluminum pans at a heating rate of 10 °C min^{-1} and a cooling rate of 2 °C min^{-1}. Two-point calibration using indium and tin was carried out to check the temperature axis and heat flow of the equipment.

2.8. Fourier transformation infrared (FTIR) spectroscopy

FTIR spectra were collected by a Nicolet-Magna FT-IR 750 spectrometer in the range from 4000 to 350 cm^{-1}, with a resolution of 4 cm^{-1} at ambient conditions.

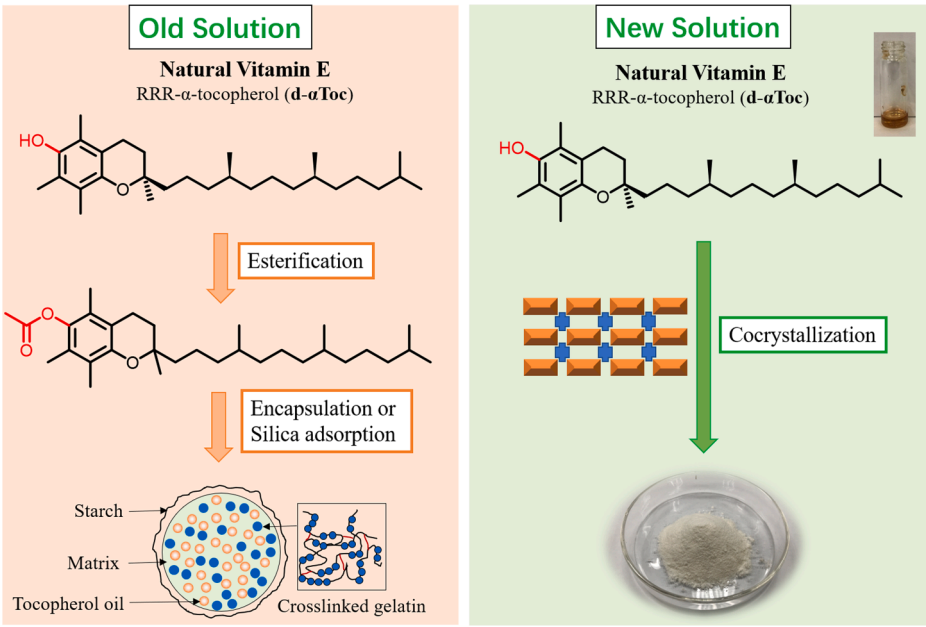

Fig. 1. Chemical structure of **d-αToc**. Esterification and encapsulation are needed to incorporate oily Vitamin E in commercial products.

2.9. Powder density measurements

Bulk and tap density were conducted on two edible cocrystals. In the measurement of bulk density, approximately 100 g of the test sample (m) were gently introduced into a dry graduated cylinder of 250 mL without compacting, and read the unsettled apparent volume (V_0) to the nearest graduated unit. The bulk density is calculated in using the formula m/V_0. In the case of tap density, after sample introduction, nominally 250 taps are needed before reading.

2.10. Stability study

Thermo stability was conducted at 60 °C and illumination stability was conducted at 5000 lx/25 °C. Oily **d-αToc** and cocrystal **d-αToc·L-Pro** powder were taken out at various intervals during exposure (thermal stability at 0, 5, 10, 20, 30 days and illumination stability at 0, 5, 10, 20 days). After that, both cocrystals **d-αToc·L-Pro** and **d-αToc·Bet** were subjected to accelerated stability (40 °C/75%RH) and long-term stability (25 °C/60%RH). The assay of **d-αToc** were determined at various intervals (accelerated stability at 0, 1, 2, 3, 6 months and long-term stability at 0, 3, 6, 9, 12 months). The packing material is polyester/aluminum/polyethylene medicinal composite bag.

2.11. Gummy candies preparation and stability study

Gummy candies were prepared according to the following formulation: 0.2% w/w Vitamin E (about 1200 mg equivalent to **d-αToc**), 2.5% w/w gelatin, 34.6 w/w sucrose, 56.8% w/w glucose syrup, 0.4% w/w citric acid. Firstly, glucose syrup, sugar and water were mixed and heated until complete dissolution. Then, the gelatin was dissolved in boiling water and added into the glucose syrup solution. Finally, citric acid and Vitamin E were added and the solution was cooled down. The gummy candies were subjected to accelerated stability (40 °C/75%RH) and the assay of **d-αToc** were determined at 1, 1/2, 3 and 6 months.

2.12. Pharmacokinetic experiments

To compare the bioavailability of different Vitamin E forms, pharmacokinetics study was conducted on cocrystal **d-αToc·L-Pro,** cocrystal **d-αToc·Bet**, **d-αToc** acetate and **d-αToc** succinate. The four Vitamin E samples were dispersed homogeneously in 0.5% CMC-Na (sodium carboxymethylcellulose) and 0.5% SDS (sodium dodecyl sulfate) aqueous solution to get the suspension of 8 mg/mL of **d-αToc**. 24 male Sprague-Dawley rats weighing 220–250 mg were randomly allocated into four groups (6 rats in each group). Each received gavage administration at a dose of 80 mg/kg body (expressed as **d-αToc** equivalents). The rats were maintained on a vitamin E-free AIN-76A diet for one week and fasted overnight before drug administration. After administration, about 200 μL of blood sample was collected into heparinized tubes at 0, 1, 2, 3, 4, 6, 8, 10, and 24 h. Plasma was immediately separated by centrifugation (10 °C, 10,000 g, 5 min) using a refrigerated table top centrifuge and kept frozen at −20 °C until analysis. Plasma samples (100 μL) were extracted by adding 200 μL ethanol containing 1% sodium ascorbate and, subsequently, 1 mcccccccccccL hexane. After vortexing for 1 min and centrifuging for 5 min (10000 rpm), 0.8 mL of the hexane layer was collected, dried using N_2, and resuspended in 200 μL ethanol. This extract was analyzed using HPLC.

2.13. High performance liquid chromatography (HPLC) analysis

The content of **d-αToc** was determined by an Agilent 1260 series HPLC (Agilent Technologies), equipped with a quaternary pump (G1311C), diode-array detector (G1315D) set at 292 nm, and a 4.6 × 150 mm, 5 μm Agilent Zorbax Ecplise Plus C18 column. Mobile phase consisting of methanol and water (98/2, v/v) was run for 15 min at 1.0 mL/min. An injection of 10 μL was performed and the column temperature was set at 30 °C.

3. Results and discussion

3.1. Cocrystal design and PXRD analysis

d-αToc features a chromane ring and a hydrophobic side chain. The hydroxyl group on the chromane ring is a classic hydrogen bond donor that can be applied for cocrystal design. Coformers containing carboxylate or N_{pyr}, which are statistically more likely to interact with phenolic hydroxyl through supramolecular synthon I or synthon II, are chosen for cocrystallization (Fig. 2a). In the case of synthon I, cocrystals with 1,2-di(4-pyridyl)ethylene (**DPE**) was successfully obtained. As for synthon II, amino acids and their derivatives, which are the best-known zwitterions with high melting points, are used for cocrystallization. Rigorous trials result in two cocrystals with L-Proline (**L-Pro**) and Betaine (**Bet**). According to the result, we perceive that α-amino acid plays an important role in successful molecular packing. Neither β-amino acid like 3-pipecolic acid nor γ-amino acid like L-carnitine is able to cocrystallize with **d-αToc**.

PXRD is primarily used to confirm cocrystal formation, wherein different characteristic peaks appear (Fig. S1). As is shown in Fig. 2b, all the cocrystals display sharp peaks indicative of high crystalline material.

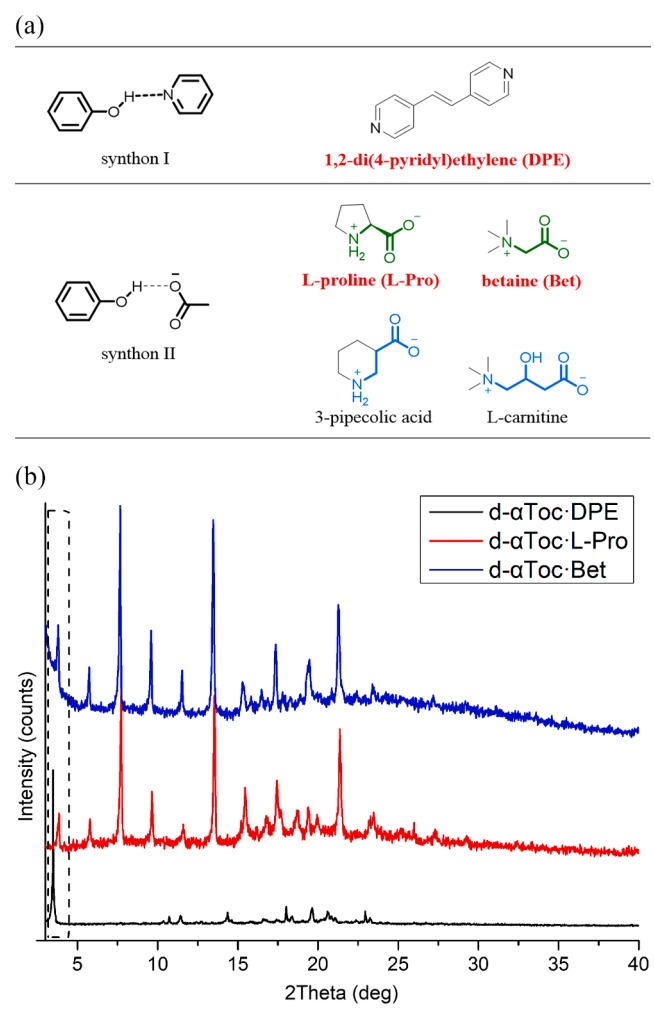

Fig. 2. (a) Crystal engineering design based on synthon I and synthon II (α-amino acid is highlighted in green and β/γ-amino acid in blue); (b) PXRD patterns of cocrystal **d-αToc·DPE**, **d-αToc·L-Pro** and **d-αToc·Bet.** (For interpretation of the references to colour in this figure legend, the reader is referred to the web version of this article.)

The characteristic peak at low angle of 3-5° reflects in a large unit cell due to the long side chain in **d-αToc** molecule. It is worth noting that PXRD patterns of **d-αToc** cocrystals with **L-Pro** and **Bet** share lots of similarities, both showing peaks at 2θ = 3.8°, 5.7°, 7.6°, 9.6°, 11.5°, 13.5°, 17.4° and 21.3°. This implies that the interaction mode and molecular arrangement in these two cocrystals are presumably the same. The introduction of small molecules served as coformers results in a high loading of **d-αToc** in cocrystals. The stoichiometry of **d-αToc** and coformers in three cocrystals were determined to be 2:1 by H-NMR (Fig. S2). Therefore, the cocrystals have a **d-αToc** loading more than 80% (w/w %), which is much higher than the encapsulation form.

3.2. Morphology and flowability characterization of cocrystals

Cocrystallization successfully affords the solidification of oily Vitamin E and free-flowing powders were obtained. Polarized light microscopy shows that **d-αToc·DPE** crystallized in plate single crystals (Fig. S3). The morphology of the two edible cocrystals, **d-αToc·L-Pro** and **d-αToc·Bet**, was revealed by SEM. Interestingly, both cocrystals are produced in spherical agglomerates with a size distribution of 50–150 μm. The agglomerates of **d-αToc·L-Pro** have high sphericity. Enlarged view of a particle reveals that the surface is extraordinarily smooth and integrated, which is quite rare in spherical crystallization of organic molecules (Kedia and Wairkar, 2019; Velivela et al., 2018). In the case of **d-αToc·Bet**, although the agglomerates show good sphericity, the surface appears to be rougher and less compact with evident void spaces. From Fig. 3(d), we can see that the agglomeration of **d-αToc·Bet** is a process of small plate crystals adhering to form spherical particles. Spherical crystallization is a good way to improve powder flowability, which is of great importance in homogeneous distribution in multivitamin blend. Herein, Carr's index was adopted to characterize the powder flowability of cocrystals **d-αToc·L-Pro** and **d-αToc·Bet**. In a free-flowing powder, the bulk density and tapped density is close, therefore, the Carr index would be small. The results are listed in

Table 1
Powder density and Carr's index of the two cocrystals.

Cocrystal	Bulk Density (ρ_T, kg/m^3)	Tap Density (ρ_B, kg/m^3)	*Carr's Index (%)
d-αToc·L-Pro	0.51	0.59	13
d-αToc·Bet	0.37	0.41	10

*Carr's Index = $100*(\rho_T-\rho_B)/\rho_T$

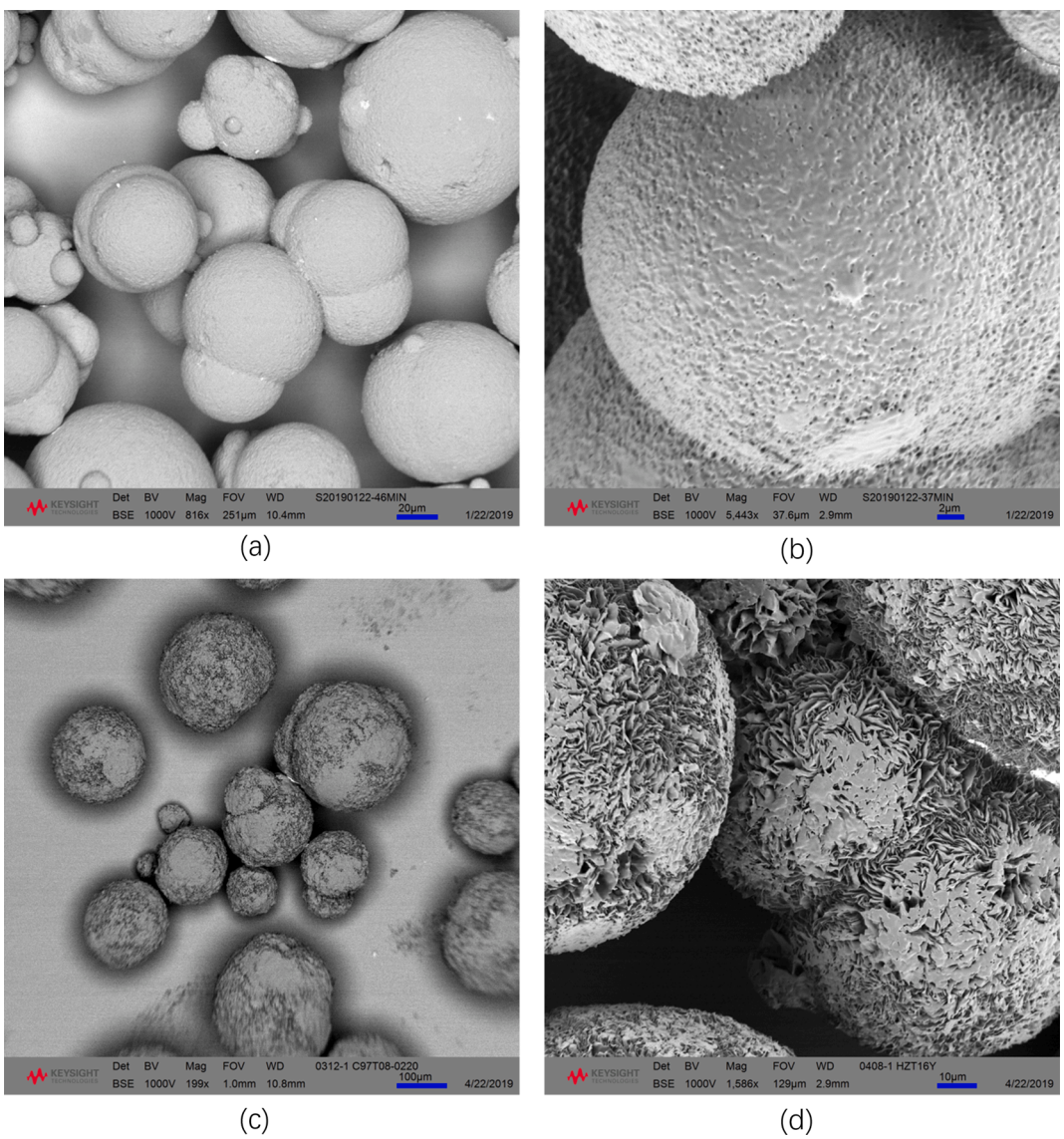

Fig. 3. Spherical agglomerates in cocrystals (a) **d-αToc·L-Pro** and (c) **d-αToc·Bet.** Enlarged view of the sphere surface in (b) **d-αToc·L-Pro** and (d) **d-αToc·Bet**.

Table 1. Both cocrystals falls within the range of 5–15, which indicates excellent flowability.

3.3. Single crystal structure

Single crystals are difficult to be obtained due to the long alkane chain in **d-αToc**. Fortunately, plate single crystal of **d-αToc·DPE** was grown when cooling at −20 °C. The crystal structure was determined and the crystallographic data is shown in Table S1. An asymmetric unit contains one **DPE** molecule and two **d-αToc** molecules, which are connected through synthon I to form a trimer. The non-polar alkyl chains are prone to be assembled together due to strong hydrophobic interactions. Along *a* axis (Fig. 4a), we can clearly see that the hydrophobic tails (yellow) of **d-αToc** are facing one side, and the hydrophilic ring on the other side, forming layers of **d-αToc** and **DPE** molecules. In this way, the molecular arrangement resembles the lamellar micelle that is usually encountered in the self-assembled structure of a surfactant. In addition to the molecular packing, we also paid particular attention to the molecular conformation. The structure and absolute configuration of **d-αToc** have been previously determined by optical rotation and NMR, (Mazzini et al., 2009; Singh et al., 2017) which however is not able to provide accurate information. This is the first time that the crystal structure of **d-αToc** was resolved. The two **d-αToc** molecules in the asymmetric unit adopt different side chain conformations in terms of the dihedral angle of O1-C1-C14-C15 (O1′-C1′-C14′-C15′). The epoxy group (C1-O1) and the phytyl side chain (C14-C15) are *gauche* oriented in one molecule and *trans* oriented in the other (Fig. 4b). The two different conformations support the previous finding that **d-αToc** are fairly flexible mostly at C1-C14 where the phytyl chain is linked to chroman nucleus (Witkowski and Wawer, 2002).

3.4. Vibrational spectra

IR spectra was further utilized to shed some light on the driving force behind the solidification. IR spectroscopy has been widely used in studying H-bond. Sharp peak at 3463 cm^{-1} (**d-αToc**) is representative of the O-H stretching in **d-αToc** molecule. In cocrystal **d-αToc·DPE**, the peak was red-shifted to 3214 cm^{-1} (Fig. S4a). Red-shifted broad band at 3438 cm^{-1} and 3341 cm^{-1} appears in cocrystal **d-αToc·L-Pro** and **d-αToc·Bet** respectively (Fig. S4b), which indicate that the phenolic hydroxyl group is involved in hydrogen bonding with coformers. Moreover, characteristic peaks at 1624 cm^{-1} and 1560 cm^{-1} in **L-Pro**, which is assignable to the COO— asymmetric stretching and the NH_2 + scissoring vibration respectively, are merged into a single peak at 1625 cm^{-1} in cocrystal. And characteristic peak at 1622 cm^{-1} assignable to the COO— asymmetric stretching in **Bet** is shifted to 1651 cm^{-1} in its cocrystal.

3.5. Thermal analysis of cocrystals

Cocrystallization significantly increases the melting point of **d-αToc**. DSC patterns are shown in Fig. 5. **d-αToc·DPE** melts at about 53 °C and an additional endothermic peak with the onset temperature of 29 °C can be observed before melting point. When heating–cooling-reheating cycle was conducted, an exothermic peak at 14 °C and the repeated occurrence of endothermic peak at 29 °C indicate that the phase

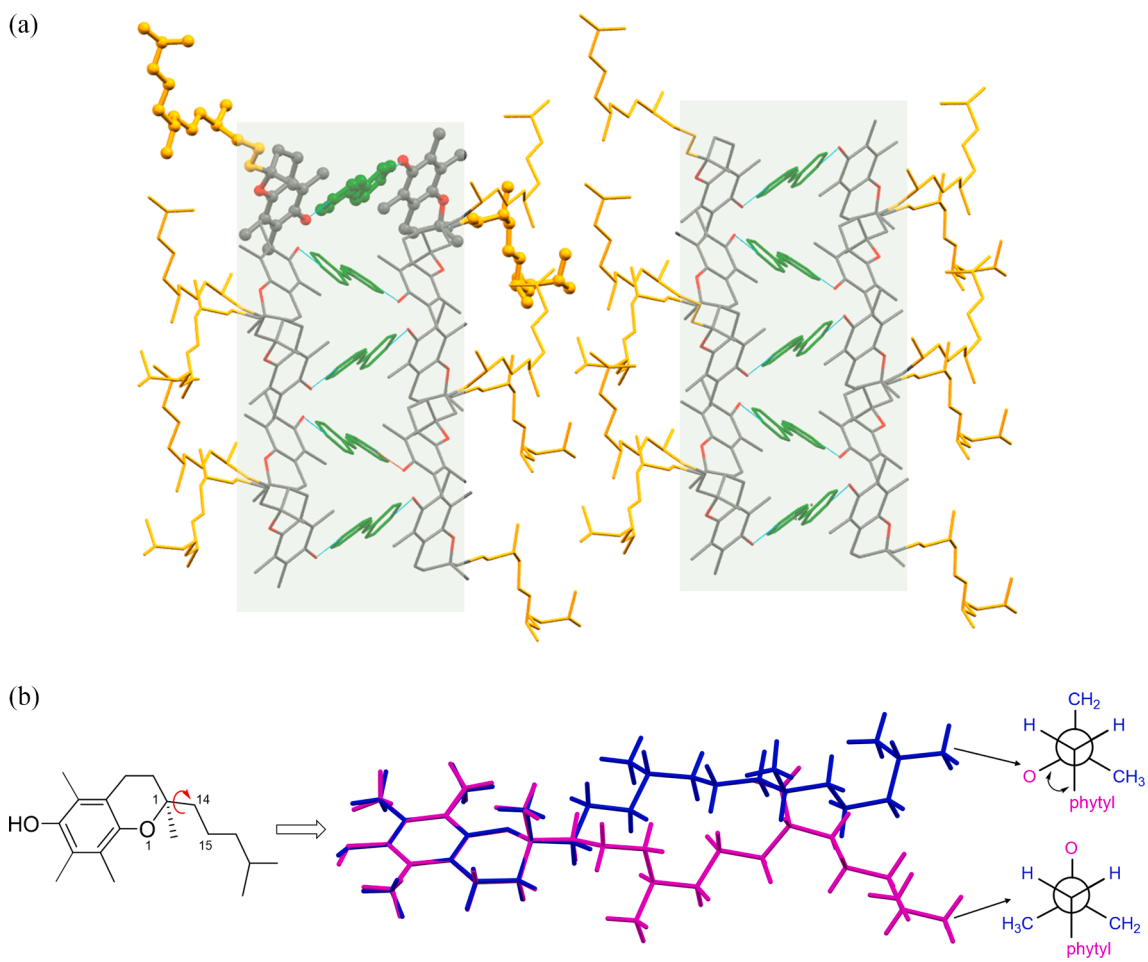

Fig. 4. (a) Crystal packing along a axis, resembling the lamellar micelle. For clarification, hydrogen atoms are omitted. (b) different gauche/trans conformation in two **d-αToc** molecules in the asymmetric unit.

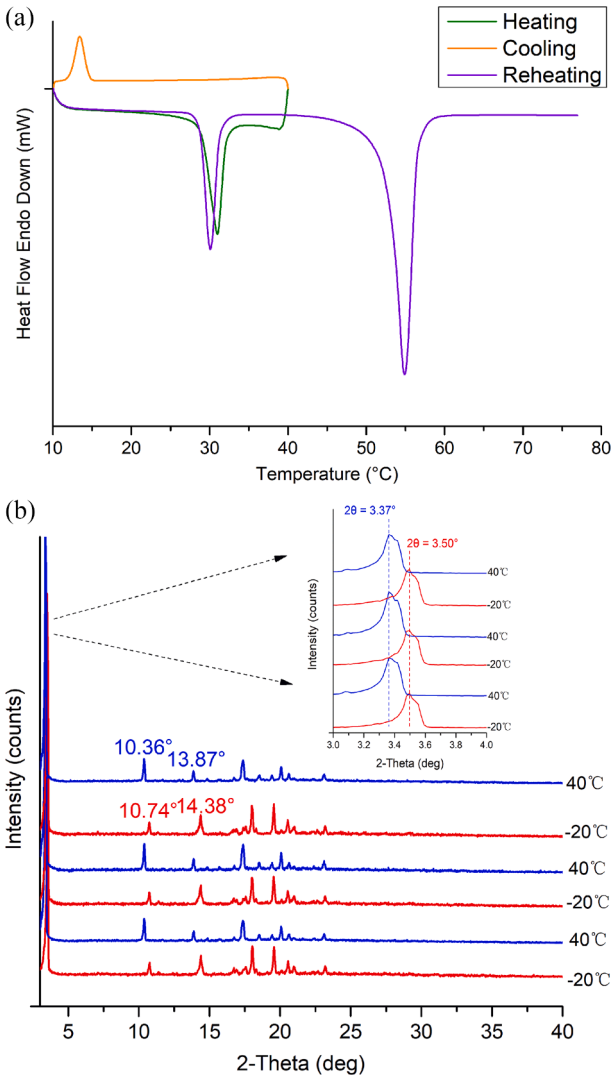

Fig. 5. (a) Heating-cooling-reheating cycle of cocrystal **d-αToc·DPE** (d) changes in PXRD patterns before and after phase transition.

transition is reversable. This transition was further verified by VT-PXRD and SXRD. As is shown in Fig. 5b, there are some small differences in the PXRD patterns before and after phase transition. When heated from −20 °C to 40 °C, diffraction peaks at 3.50°, 10.74° and 14.38° shift to lower angles of 3.37°, 10.36°, and 13.87° respectively. Single crystal determination after transition demonstrated that there was no big difference in the interaction mode and molecular arrangement, but a slightly offset between the layers can be observed (Fig. S5). We perceive that the phase transition is presumably induced by conformational changes in the alkyl chain of **d-αToc**, which is highly flexible. Interestingly, the other two isomeric cocrystals of **d-αToc**, **d-αToc·L-Pro** and **d-αToc·Bet**, also show a phase transition at 45 °C and 41 °C respectively, despite of the significant different melting point of these two cocrystals (Fig. S6). Cocrystal **d-αToc·L-Pro** melts at about 73 °C and cocrystal **d-αToc·Bet** has a melting point up to 106 °C. The much higher melting point of **d-αToc·Bet** can be attributed to its stronger intermolecular interaction, which is also reflected in the greater redshift of O-H stretching in IR spectra (3463 cm^{-1} to 3341 cm^{-1}). Likewise, when conducting a heating–cooling-reheating cycle, the phase transition in **d-αToc·L-Pro** and **d-αToc·Bet** is reversible. However, the PXRD patterns before and after this transition temperature are essentially the same, which indicates that the conformational change in **d-αToc·L-Pro** and **d-αToc·Bet** dose not induce the changes in unit cell (Fig. S6). This is also reflected in the enthalpy of the phase transition in these cocrystals. The enthalpy of the phase transition is 1.3 g/J in **d-αToc·L-Pro** and 5.4 J/g in **d-αToc·Bet**, which is much smaller compared to 16.0 J/g in **d-αToc·DPE**.

3.6. Stability studies

Both thermo (60 °C for one month) and illumination stability (5000 lx for 20 days) were investigated for oily **d-αToc** and cocrystal **d-αToc·L-Pro** (Fig. 6). The result shows that the assay value of **d-αToc** decreased to 77.3% after one month at 60 °C and 88.5% after 20 days under illumination. However, the **d-αToc** content in cocrystal is still up to 95.4% and 97.4% respectively. Furthermore, two edible cocrystals **d-αToc·L-Pro** and **d-αToc·Bet** were subjected to accelerated stability (40 °C/75%RH) and long-term stability (25 °C/60%RH) investigation. No obvious changes in content were observed in both conditions (Table S2). To further evaluate its stability in real application situations, gummy candy was selected as a food model which was becoming increasingly popular as a type of vitamin supplement. Gummy candies containing cocrystal **d-αToc·L-Pro** were prepared and the assay of **d-αToc** was measured over time under accelerated condition (40 °C/75% RH). The result shows that there is no decrease of **d-αToc** after 6 months (Table S3). Therefore, high stability of **d-αToc** in its original form was successfully achieved by cocrystallization. Prevention of oxygen penetration due to compact spherical crystallization and the hydrogen bond involved in the reactive phenolic hydroxy group are supposed to contribute to cocrystal stability.

3.7. Bioavailability studies

Finally, the bioavailability study of **d-αToc** and its cocrystals was carried out. There have been a lot of reports in terms of the effect of different chemical forms of Vitamin E on its bioavailability (van Kempen et al., 2016). The esterified form of Vitamin E has a lower bioavailability than the free form, because it is more difficult to incorporate into mixed micelles and has to be hydrolyzed first before absorption. However, esterified forms are generally used in commercial products due to the higher stability. In this study, stable solid forms of **d-αToc** are developed and would have a potential advantage on absorption. We compare the plasma concentrations of **d-αToc** after ingestion of **d-αToc** acetate, **d-αToc** succinate, cocrystal **d-αToc·L-Pro**, and cocrystal **d-αToc·Bet** on rats. Samplings were made at 0, 1, 2, 3, 4, 6, 8, 10, 24 h. Fig. 7 shows the mean plasma concentrations of **d-αToc** versus time profiles. Succinate form has the lowest C_{max} of 9.0 μg/mL and acetate form is slightly higher. Compared with the succinate form, two cocrystals display an obvious increase in C_{max} of 45.6% for **d-αToc·L-Pro** and 55.6% for **d-αToc·Bet**. Therefore, the bioavailability of **d-αToc** was enhanced by cocrystalliztion, which would bring additional health benefits as nutrient supplements.

4. Conclusion

In conclusion, we have successfully tuned oily Vitamin E into crystal Vitamin E by hydrogen-bond driven cocrystallization. All the cocrystals are produced in solid state at room temperature, in which cocrystal with **Bet** has a melting point of 110 °C higher than the starting material. Single crystal structure of **d-αToc** was firstly uncovered and the hydrogen bond O—H···N_{pyr} was validated. The three cocrystals with **d-αToc** display a phase transition before melting due to the conformational changes in the alkyl chain. Interestingly, cocrystals with **Pro** and **Bet** are generated in spherical agglomerates with good power flowability, which would be particularly beneficial to homogeneous mixing during its application. Stability study show that the cocrystals of Vitamin E, although in its free form, has no stability issue. Last but not the least, compared with the esterified forms, a significant bioavailability improvement of **d-αToc** can be achieved. The results of the

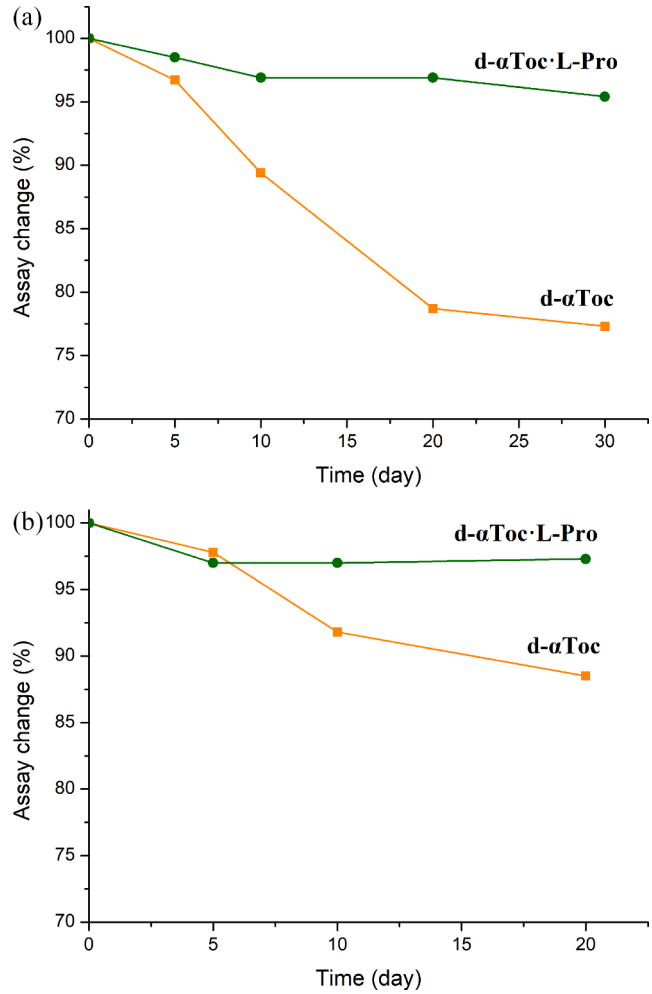

Fig. 6. Assay changes of **d-αToc** in (a) thermal and (b) illumination stability studies (The content of **d-αToc** at 0 day was set as 100%).

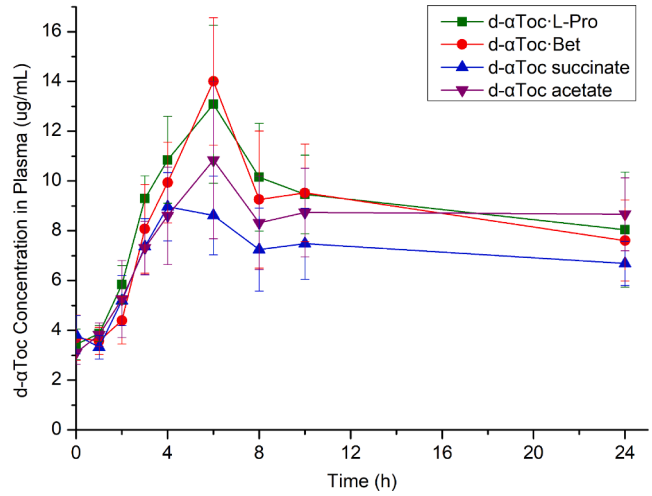

Fig. 7. Plasma **d-αToc** concentration–time profiles of **d-αToc** acetate, **d-αToc** succinate, cocrystal **d-αToc·L-Pro**, and cocrystal **d-αToc·Bet**.

current work demonstrated a great advantage of **d-αToc** cocrystals over the commercial esterified Vitamin E forms. Therefore, **d-αToc** cocrystals should be a superior choice of natural Vitamin E source in nutrient supplement. Cocrystallization technique is proved be to a more effective method for the solidification and stabilization of Vitamin E, which spares a large quantity of acetic ester and significantly saves the production cost. Further researches will be conducted to explore its application on synthetic Vitamin E, which is widely used in feed industries.

CRediT authorship contribution statement

Bingqing Zhu: Conceptualization, Methodology, Investigation, Visualization. **Qi Zhang:** Investigation. **Liye Lu:** Validation. **Junjie Bao:** Investigation. **Xiaoyi Rong:** Investigation. **Jian-Rong Wang:** Conceptualization. **Xuefeng Mei:** Supervision.

Declaration of Competing Interest

The authors declare that they have no known competing financial interests or personal relationships that could have appeared to influence the work reported in this paper.

Appendix A. Supplementary material

Supplementary data to this article can be found online at https://doi.org/10.1016/j.ijpharm.2020.120057.

References

El Hadi, H., Vettor, R., Rossato, M., 2018. Vitamin E as a Treatment for Nonalcoholic Fatty Liver Disease: Reality or Myth? Antioxidants (Basel) 7, 12.
Sebastian Larion, M.D., Sandeep Khurana, M.B.B.S., 2018. Clinical Studies Investigating the Effect of Vitamin E Therapy in Patients with NASH. Clin. Liver Dis. 11, 16–21.
Mangialasche, F., Westman, E., Kivipelto, M., Muehlboeck, J.S., Cecchetti, R., Baglioni, M., Tarducci, R., Gobbi, G., Floridi, P., Soininen, H., Kloszewska, I., Tsolaki, M., Vellas, B., Spenger, C., Lovestone, S., Wahlund, L.O., Simmons, A., Mecocci, P., AddNeuroMed, C., 2013. Classification and prediction of clinical diagnosis of Alzheimer's disease based on MRI and plasma measures of alpha-/gamma-tocotrienols and gamma-tocopherol. J. Intern. Med. 273, 602–621.
Ulatowski, L., Parker, R., Warrier, G., Sultana, R., Butterfield, D.A., Manor, D., 2014. Vitamin E is essential for Purkinje neuron integrity. Neuroscience 260, 120–129.
Player, M.E., Kim, H.J., Lee, H.O., Min, D.B., 2006. Stability of α-, γ-, or δ-Tocopherol during Soybean Oil Oxidation. J. Food Sci. 71, C456–C460.
Lv, S., Zhang, Y., Tan, H., Zhang, R., McClements, D.J., 2019. Vitamin E Encapsulation within Oil-in-Water Emulsions: Impact of Emulsifier Type on Physicochemical Stability and Bioaccessibility. J. Agric. Food. Chem. 67, 1521–1529.
Reboul, E., 2017. Vitamin E Bioavailability: Mechanisms of Intestinal Absorption in the Spotlight. Antioxidants (Basel) 6.
Desmarchelier, C., Tourniaire, F., Preveraud, D.P., Samson-Kremser, C., Crenon, I., Rosilio, V., Borel, P., 2013. The distribution and relative hydrolysis of tocopheryl acetate in the different matrices coexisting in the lumen of the small intestine during digestion could explain its low bioavailability. Mol. Nutr. Food Res. 57, 1237–1245.
Bruno, R.S., Leonard, S.W., Park, S., Zhao, Y.Y., Traber, M.G., 2006. Human vitamin E requirements assessed with the use of apples fortified with deuterium-labeled alpha-tocopheryl acetate. Am. J. Clin. Nutr. 83, 299–304.
Gangurde, A.B., Ali, M.T., Pawar, J.N., Amin, P.D., 2016. Encapsulation of vitamin E acetate to convert oil to powder microcapsule using different starch derivatives. J. Pharm. Invest. 47, 559–574.
Duggirala, N., Perry, M., Almarsson, O., Zaworotko, M., 2016. Pharmaceutical cocrystals: along the path to improved medicines. Chem. Commun. (Camb.) 52, 640–655.
Wang, J.-R., Yu, Q., Dai, W., Mei, X., 2016. Drug–drug co-crystallization presents a new opportunity for the development of stable vitamins. Chem. Commun. 52, 3572–3575.
Zhu, B., Wang, J.-R., Zhang, Q., Mei, X., 2016. Improving Dissolution and Photostability of Vitamin K3 via Cocrystallization with Naphthoic Acids and Sulfamerazine. Cryst. Growth Des. 16, 483–492.
Aakeroy, C.B., Wijethunga, T.K., Benton, J., Desper, J., 2015. Stabilizing volatile liquid chemicals using co-crystallization. Chem. Commun. 51, 2425–2428.
McKellar, S.C., Kennedy, A.R., McCloy, N.C., McBride, E., Florence, A.J., 2014. Formulation of Liquid Propofol as a Cocrystalline Solid. Cryst. Growth Des. 14, 2422–2430.
Sheldrick, G. M., SANIT and XPREP. 5.1 ed.; Siemens Industrial Automation Inc.: Madison, WI, 1995.
Sheldrick, G.M., 1997. SADABS. University of Gottingen, Gottingen, Germany.
Sheldrick, G.M., 2015. SHELXT - Integrated space-group and crystal-structure determination. Acta Cryst. 71, 3–8.
Kedia, K., Wairkar, S., 2019. Improved micromeritics, packing properties and compressibility of high dose drug, Cycloserine, by spherical crystallization. Powder Technol. 344, 665–672.
Velivela, S., Pati, N.B., Ramamohan Gupta, V., 2018. Spherical crystallization: a novel technique in drug particle designing. World J. Pharm. Pharm. Sci. 7, 363–376.

Mazzini, F., Pescitelli, G., Di Bari, L., Netscher, T., Salvadori, P., 2009. Circular dichroism of tocopherols versus tocotrienols. Chirality 21, 35–43.
Singh, G., Sachdeva, R., Rai, B., Saini, G.S.S., 2017. Structure and vibrational spectroscopic study of alpha-tocopherol. J. Mol. Struct. 1144, 347–354.
Witkowski, S., Wawer, I., 2002. 13C NMR studies of conformational dynamics in α-tocopherol esters in solution and solid state. J. Chem. Soc. Perkin Trans. 2, 433–436.
van Kempen, T., Reijersen, M.H., de Bruijn, C., De Smet, S., Michiels, J., Traber, M.G., Lauridsen, C., 2016. Vitamin E plasma kinetics in swine show low bioavailability and short half-life of all-rac-alpha-tocopheryl acetate. J. Anim. Sci. 94, 4188–4195.